

Non-linearity and frequency shifts of nuclear magnetic spin-noise [☆]

Martin Nausner ^a, Judith Schlagnitweit ^a, Vilko Smrečki ^b, Xu Yang ^c, Alexej Jerschow ^c, Norbert Müller ^{a,*}

^a Institute of Organic Chemistry, Johannes-Kepler University Linz, Altenbergerstraße 69, A-4040 Linz, Austria

^b NMR Center, Rudjer Bošković Institute, Bijenička 54, HR-10000 Zagreb, Croatia

^c Chemistry Department, New York University, New York, NY 10003, USA

ARTICLE INFO

Article history:

Received 20 November 2008

Revised 13 January 2009

Available online 21 January 2009

Dedicated to Richard R. Ernst on the occasion of his 75th birthday.

Keywords:

Spin-noise

Nyquist noise

Sensitivity

Tuning

Radiation damping

ABSTRACT

We have systematically investigated the line shapes observed in proton nuclear spin-noise spectra which depend in a complex way on the properties of the resonance circuit, the number of spins present, transverse relaxation, inhomogeneous broadening, and radiation damping. Using highly sensitive high resolution probes these dependencies are investigated by way of high resolution ¹H noise power NMR spectra of liquid samples. Significant deviations from intuitive expectations are observed. Simulations based on an adapted Nyquist noise equation are used to understand and interpret the experimental findings.

© 2009 Elsevier Inc. All rights reserved.

1. Introduction

The phenomenon of spin-noise was predicted by Bloch in 1946 [1], but at the time could not be detected. Sleator and Hahn were able to measure spin-noise for the first time using a solid sample at liquid helium temperature [2,3]. Later, Ernst and McCoy demonstrated that spin-noise was also observable at ambient temperature with a commercial liquid-state NMR spectrometer [4]. An independent report about such measurements was presented by Guéron [5], who also developed a viable coupled resonator model [6]. Nuclear spin-noise was also detected optically using a technique based on Faraday rotation [7]. Recently, nuclear spin-noise was detected in the presence of magnetic field gradients along different directions and exploited to reconstruct a two-dimensional image of the cross section of a phantom without the use of radio-frequency irradiation [8]. Due to the weakness of the spin-noise signal, which originates from a system in equilibrium, as opposed to the signal obtainable from pulsed NMR, where manipulated states are generally not in equilibrium, the applications of this phenomenon are currently limited. One can expect spin-noise detected NMR to gain some importance in practical applications in selected cases, in particular with small samples

(on the order of 10⁷ or fewer nuclear spins). Although this is an experimental regime that is currently several orders of magnitude below the detection threshold, it is not out of the question that advanced techniques, for example based on optical detection may make this feasible. Electron spin-noise from paramagnetic centers on surfaces has been successfully detected recently using tunneling current measurements [9]. With cryogenically cooled probes, the observation of nuclear spin-noise phenomena has become relatively straightforward with a large numbers of spins (~10²⁰ to 10²²) [10,11], however the detection with state-of-the-art standard high resolution probes is also possible albeit at somewhat longer accumulation times.

The original motivation for the work presented here was the assessment of the fundamental properties of spin-noise which may be of relevance for future spectroscopic applications.

2. Theory

The total power P of the spin-noise signal at Larmor frequency $\omega_s/2\pi$ is given by Sleator et al. [3] as

$$P = \frac{\pi Q \omega_s N \gamma^2 \hbar^2}{V_c} \quad (1)$$

where Q is the quality factor of the rf-circuit, N is the number of spins of gyromagnetic ratio γ in a coil of volume V_c . The remarkable coincidence of this power with the power expected from spontaneous emission enhanced by the radiation density in a tuned cavity

[☆] Part of this work was presented first at the ENC 2008 (March 9–14, 2008, Asilomar California) and EUROMAR 2008 (July 6–11, 2008, St. Petersburg, Russia).

* Corresponding author. Fax: +43 732 2468 8747.

E-mail addresses: norbert.mueller@jku.at, norbert.mueller@jk.uni-linz.ac.at (N. Müller).

led to the conclusion that spin-noise and spontaneous emission were part of the same mechanism [3]. Houlton and Ginsberg discuss this relationship in further detail and invoke a mechanism based on virtual photons to complete the connection [12,13]. Overall, however, other than with the power comparison, it is difficult to draw a direct connection between these two phenomena.

While this equation describes the total spin-noise power, one needs to resort to equations based on the Nyquist noise [14] relationship modified for the presence of resonating spins in order to describe line shapes. In the formulation of McCoy and Ernst [4] the line shape of the spin-noise power signal is described by

$$W(\omega) = q \frac{1 + a(\Delta\omega)\lambda_r^0}{[1 + a(\Delta\omega)\lambda_r]^2 + [d(\Delta\omega)\lambda_r + 2Q\Delta\omega_c/\omega_c]^2} \quad (2)$$

where $\Delta\omega$ is the resonance offset, $\Delta\omega_c$ is the offset from the rf-circuit's tuning center frequency ω_c , q is a frequency independent factor depending on the circuit resistance and temperature,

$$\lambda_r = 1/T_{rd} = \frac{1}{2} \eta Q \gamma \mu_0 M_z \quad (3)$$

is the radiation damping rate [15–18], with M_z being the z-magnetization, η the filling factor, and μ_0 the permeability of free space. The difference between sample temperature T_s and circuit temperature T_c is taken into account via

$$\lambda_r^0 = \lambda_r \frac{T_s}{T_c} = \lambda_r \vartheta \quad (4)$$

The temperature ratio ϑ makes a substantial difference for cryogenically cooled probes as will be seen below. The absorptive $a(\Delta\omega)$ and dispersive $d(\Delta\omega)$ line shapes are responsible for the different appearances of the spectra under the influence of various homogeneous and inhomogeneous interactions. By substituting entire multi-resonance spectra for these line shapes spin-noise spectra of complex systems can be simulated.

We further note that the appearance of the spectra predicted from Eq. (2) and measured experimentally is similar but not identical to the appearance of spectra with small flip angle pulse excitation in the presence of radiation damping [17].

3. Experimental

Results from two differently equipped NMR spectrometers are shown in this paper to demonstrate the different regimes and the instrument dependence of the spin-noise phenomena (to ensure generality, qualitative tests were run on a larger number of spectrometers and probes).

Spin-noise NMR spectra used in the present Article were collected and processed using the following instruments, parameters and protocols unless otherwise noted:

In order to collect spin-noise data using a Bruker cryo-probe we turn off the mains supply of the proton amplifier, disconnect the BNC-connector for the input to the proton amplifier and replace it by a 50 Ω terminator. The terminators are a precaution – we have also successfully recorded spin-noise without them. For non-cryo-probes we proceed as follows: The ^1H power amplifier's mains supply was switched off and the ^1H rf-pulse cable coming from the power amplifier was disconnected from the back of the pre-amplifier, and a 50 Ω terminator was attached to the pre-amplifier instead.

Data were collected using a pseudo 2D pulse sequence (without pulse) collecting one noise block per row at a spectral width of 10 ppm with the carrier set to 5.5 ppm. A total of 1024 blocks (or more for weaker spin-noise cases) were typically collected in this way, Fourier transformed individually to complex-valued (phase sensitive) spectra; i.e. $S(\omega) = u(\omega) + i v(\omega)$ individually, and converted to power spectra, i.e. $P(\omega) = u^2(\omega) + v^2(\omega)$, using the

TopSpin command *xf2* with parameter *mc2 = ps*. Finally, the rows were summed up (TopSpin command *f2sum*).

The following NMR spectrometers were used to obtain the data shown in this Article: A Bruker DRX 500 (11.7 T) instrument with a 5 mm high resolution triple resonance (TXI,H,C,N) cryo-probe (sample temperature 298.3 K, rf-coil temperature 30.5 K) with an internal z-gradient coil, Bruker AV600 (14 T) with a 5 mm high resolution triple resonance broadband (TBI,H,C, BB) probe (sample and rf-coil temperature 298.3 K) with a built-in z-gradient coil.

The spin-noise simulations according to Eq. (2) were performed with $Q = 1850$, an intrinsic linewidth at half height of 3.5 Hz for iso-propanol and H_2O , and 2.5 Hz for acetone (for acetone and iso-propanol, these were determined from the measurement of the linewidths of the ^{13}C -satellites). $\lambda_r = 31 \text{ s}^{-1}$ for 90% H_2O , 22.9 s^{-1} for 90% acetone, 23.6 s^{-1} for 90% iso-propanol, and the Lorentzian lineshapes were used for $a(\Delta\omega) = \frac{1/T_2}{(1/T_2)^2 + (\Delta\omega)^2}$ and $d(\Delta\omega) = \frac{\Delta\omega}{(1/T_2)^2 + (\Delta\omega)^2}$. In the simulations involving the application of magnetic field gradients, a top-hat lineshape was convoluted with the intrinsic Lorentzian lineshape.

4. Results and discussion

In Fig. 1, we show a ^1H spin-noise NMR spectrum of a solution of 80% iso-propanol in DMSO obtained at an early stage of this investigation. The sample was chosen to provide tests for the dynamic range, linearity and resolution of spin-noise spectra, as well as, for the fact that the spin density is especially high due to the six methyl protons. 10% DMSO- d_6 was included to provide for a stable lock signal during the long data collection periods, thus allowing us to obtain the highest resolution spin-noise spectra so far reported as can be appreciated from the narrow lines in Fig. 1. A few surprising facts are immediately visible from this spectrum.

(1) Although this is a power spectrum (the accumulation of phase sensitive spectra leads to cancellation of the noise response) it exhibits a dispersion-like line-shape (in particular in the CH_3 -region), which is reminiscent of an ill-phased pulse spectrum. It should be noted, however, that the baseline in spin-noise spectra does not represent zero amplitude, but is determined by the total (thermal) circuit noise power.

(2) The peak areas do not reflect the number of nuclei, e.g., the area of the OH proton signal (at ~ 4.9 ppm) is much larger than the one of the CH_3 -groups (at ~ 1.1 ppm).

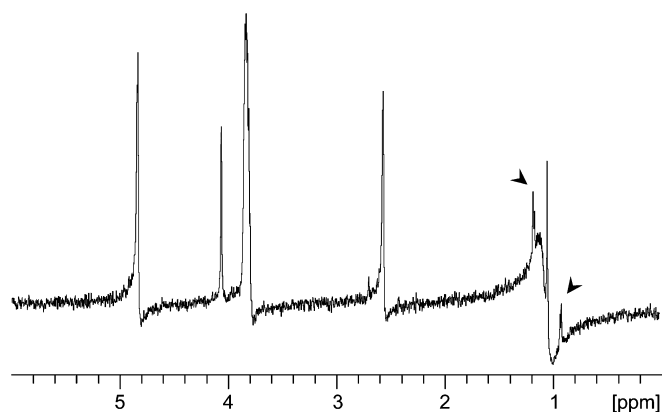


Fig. 1. 500 MHz ^1H spin-noise NMR spectrum (4 k accumulated data blocks of 8 k data points) of a mixture of 10%(v/v) DMSO, 80%(v/v) iso-propanol and 10%(v/v) DMSO- d_6 . The arrows indicate the positions of the ^{13}C -satellites of the CH_3 signal.

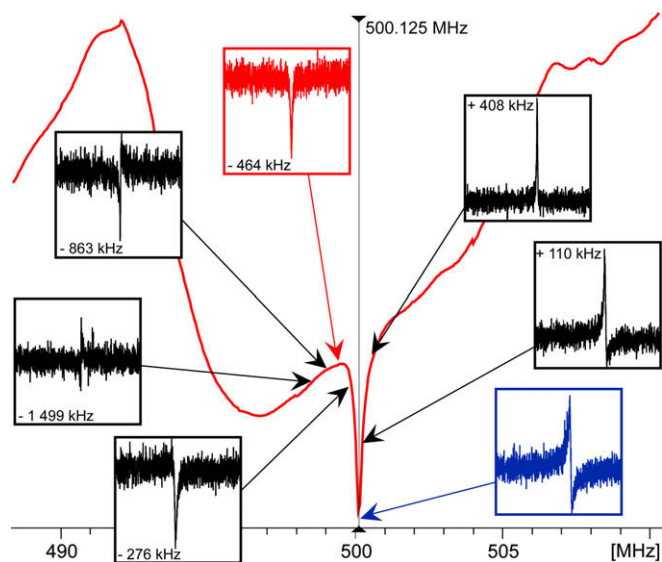


Fig. 2. Tuning dependence of the spin-noise signal of H_2O (10% $^2\text{H}_2\text{O}$) on a 500 MHz cryogenically cooled TXI probe. The large red curve is the “wobble” curve as displayed by the tuning routine (“wobb”) of the Bruker TopSpin software. The small inset spectra connected to the tuning curve by arrows, which indicate the tuning offsets, display the changing line shapes of the spin-noise power spectra. The data were acquired using the general parameters and protocol given in the Experimental Section (but with only 512 noise blocks of 4 k data points accumulated for each). The line shape at the conventional tuning optimum, shown in blue color, has a dispersive character. The “dip” line shape in the red inset spectrum is not found as predicted by Eq. (2) at the minimum position of the tuning curve but at an offset of -464 kHz. The tuning offset was adjusted manually using the tuning screw on the probe—for each setting the “matching” was readjusted to give the lowest minimum of the curve.

(3) The ^{13}C -satellites of the CH_3 -groups are clearly visible, as emphasized by arrows in Fig. 1, but their amplitude exceeds by far what one would expect from this natural isotope abundance sample.

In the following we show that these observations can mostly be explained at least semi-quantitatively by the appropriate application of the theory, which was briefly outlined above.

4.1. Tuning dependence

According to Eq. (2) the spin-noise signal can be a negative deviation from the otherwise flat baseline, if the tuning frequency of the circuit ω_c is equal or close to the Larmor frequency. As can be seen from the experimentally observed tuning dependence of spin-noise illustrated in Fig. 2, this is generally not found to be true in practice. We find the “dip” line shape at a considerable offset from the normal tuning optimum determined for optimum pulse efficiency. We call the special tuning setting, where the spin-noise spectrum shows a symmetrical dip (the red spectrum in Fig. 2), the spin-noise tuning optimum (SNTO). This setting differs from the one determined by the conventional tuning procedure (“wobbling” on Bruker spectrometers), which, as it turns out, optimizes for excitation rather than detection, and where a dispersive spin-noise power line shape is found (the blue spectrum in Fig. 2) similar to the line shapes in Fig. 1. We found that the SNTO varies considerably between different probes (e.g., -470 ± 40 kHz on a 500 MHz Bruker TXI cryogenic probe and $+820 \pm 50$ kHz on a 600 MHz Bruker TBI ambient temperature probe), but it exhibits only a minor dependence on the sample properties (± 40 kHz) such as polarity and temperature. It should be noted here that the reproducibility of the tuning procedure is also limited to a similar range, given by the probe mechanics (tuning rods). We observed also some dependence of the SNTO position on the tuning of other channels on a multi-nuclear ambient temperature probe. In our experience the SNTO position has to be determined for each probe individually, since it depends on the circuit tuning characteristics and the electronic component properties, and there is no set relationship to the conventional tuning optimum. Very recently Marion and Desvaux [19] exploited this phenomenon for an alternative tuning approach for high resolution NMR probes. We corroborate their findings in Fig. 3 by reporting a nearly 50% increase of the signal-to-noise ratio (SNR) in a pulsed spectrum even of an aqueous sample under SNTO conditions. In this Figure we show the tuning dependence of the signal amplitude (a), the RMS-noise (b), and the SNR (c) of the anomeric signal (d) in pulsed spectra of aqueous sucrose in a 500 MHz cryo-probe. The zero-frequency point in these diagrams corresponds to the optimum obtained by the conventional probe tuning procedure. From Fig. 3a it can be seen that

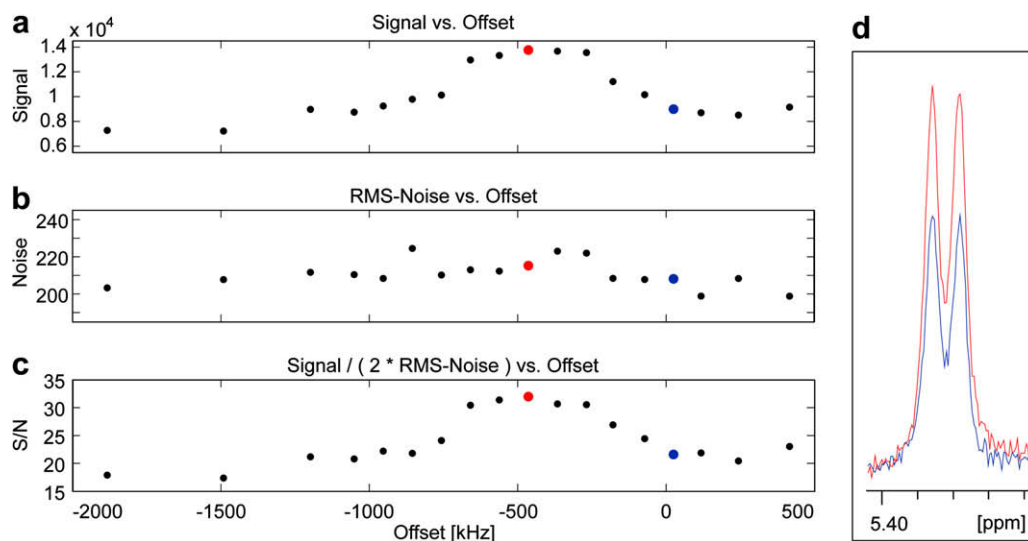


Fig. 3. Tuning dependence of the signal amplitude (a), RMS-noise level (b), and signal-to-noise ratio (c) of the anomeric doublet (d) in phase sensitive (absorptive) pulsed ^1H NMR spectra of sucrose, acquired under the following conditions: pre-saturation of the water signal for 1.5 s with an rf-power of $B_1\gamma/(2\pi) \sim 150$ Hz. For each setting of the tuning the 90° pulse width was separately calibrated and the solvent pre-saturation frequency adjusted for minimum response. A 30° pulse was used in the signal-to-noise tests to avoid accidental ADC overflow effects. The position of the tuning optimum (as determined by the spectrometer’s “wobb” routine) is at zero offset frequency emphasized by blue dots in the corresponding graphs, while the SNTO is marked by the red dots. The red and blue traces in (d) depict the anomeric doublet of sucrose at the SNTO and tuning optimum conditions, correspondingly.

the signal amplitude exhibits a broad maximum around an offset of ca. -470 kHz from the tuning optimum frequency, while the noise power in the pulsed spectrum varies only by a small amount over the tuning range (Fig. 3b). This clearly indicates that the increased SNR is due to the *increase in signal*, while the *noise level is largely unaffected*. Fig. 3d illustrates the signal increase observed on the anomeric doublet from the conventional tuning (blue trace) to SNT0 conditions (red curve). While optimizing the solvent signal suppression in these spectra we observed severe radiation damping effects at and near the SNT0. It should be noted that tuning by a network analyzer cannot be applied to current commercial cryogenically cooled probes since the pre-amplifiers are firmly attached and permanently connected to the receiver circuit and that spin-noise observation is therefore a unique non-invasive way to characterize the resonator's properties.

From inspection of the tuning curve in Fig. 2 it is also evident that the definition of a probe quality factor Q is not straightforward due to the irregular shape of the tuning curve. Modifications of Eq. (2) may help in describing non-ideal circuits with better quantitative agreement. Nonetheless to first order an estimate for the quality factor can be obtained by $Q = \nu_0/\Delta\nu$, where ν_0 is the Larmor frequency, and $\Delta\nu$ the full width at half height of the tuning dip, which may be approximated by a Lorentzian.

4.2. Non-linearity

In our previous report [8] we demonstrated the linear dependence of the spin-noise power on spin concentration. The experiments reported there were performed on a room-temperature probe at the probe's "tuning optimum" since at that time the large offset of the SNT0 had not yet been known. The apparent non-linearity of spin-noise amplitudes evidenced in Fig. 1 prompted us to reinvestigate the dependence of spin-noise power on the number of spins. In Fig. 4a spin-noise power spectra of H_2O in $^2\text{H}_2\text{O}$ under SNT0 conditions at various concentrations are shown. The spectrometer was locked to the deuterium signal and the field homogeneity was carefully adjusted to give a symmetrical Lorentzian line shape of 2.8 Hz half width in a pulsed spectrum of a 1% H_2O in $^2\text{H}_2\text{O}$ sample beforehand. From the graphs in Fig. 4a it can be readily seen that the spin-noise power spectrum changes from a positive extrusion in the noise base line via a series of complex superpositions of a narrow peak on top of a broad "dip" to a pure broad (ca. 100 Hz) "dip". The base line actually has a (fairly high) positive offset corresponding to the thermal noise background of the entire electronics. Therefore, in a spin-noise power spectrum a negative peak or "dip" represents a situation of "less than thermal noise" while a positive peak or "bump" means "more than thermal noise". The observed behavior inevitably causes non-linearity of the spin-noise power, which is most evident at high concentrations, where the effect inverts its sign. In simulations this behavior can be traced to the influence of the total z-magnetization M_z , which together with a high probe quality factor Q affects Eq. (2) by enhancing the radiation damping rate λ_r , defined in Eq. (3).

An important parameter to consider in cryo-probes is the ratio between the sample temperature and the circuit temperature $\vartheta = T_s/T_c$, introduced in Eq. (4). Assuming a Lorentzian lineshape for $a(\Delta\omega)$ and $d(\Delta\omega)$, SNT0 conditions ($\Delta\omega_c = 0$), and starting from Eq. (11) of Ref. [4], one can deduce the following condition for observing a "dip" in the spin-noise spectrum at equilibrium

$$\frac{1}{T_2}(\vartheta - 2) < \lambda_r. \quad (5)$$

For a room-temperature probe at equilibrium $\vartheta = 1$, and in such a case there is always a spin-noise "dip" under SNT0 conditions, however small. For a cryogenic probe with the sample at thermal equilibrium, one can observe both a bump (when $\vartheta > 2$, and when $1/T_2$ is

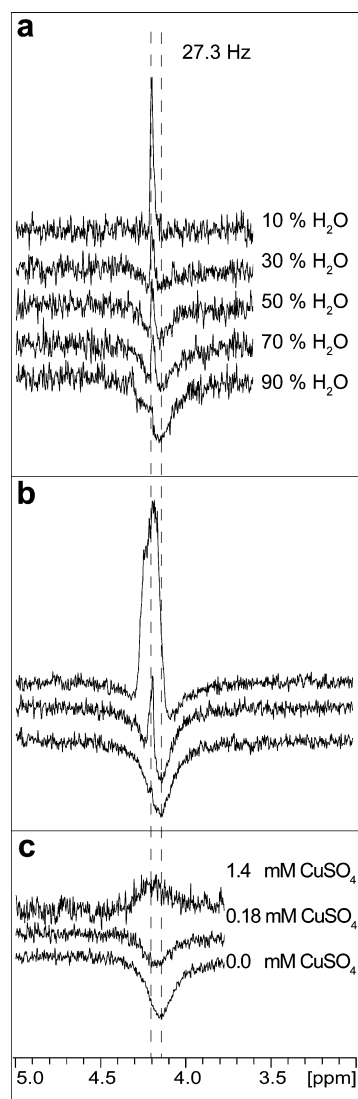


Fig. 4. Line shapes of the spin-noise signal of $\text{H}_2\text{O}/^2\text{H}_2\text{O}$ under SNT0 conditions on a 500 MHz cryo-probe. In panel (a) the dependence on H_2O concentration is shown. Panel (b) illustrates the effects of small static magnetic field gradients applied through variation of the z-shim during spin-noise acquisition on the 90% H_2O sample (the lowest trace shown was acquired without gradient). Note that a weak gradient can increase the area of the spin-noise peak. In (c) the effect of homogeneous broadening is demonstrated by addition of CuSO_4 at the indicated concentrations. 512 data blocks of 4 k data points were accumulated for (a) and 2048 data blocks of 4 k data points for (b) and (c) to compensate for the lower peak amplitudes.

larger than λ_r) as well as a dip. A similar behavior is seen when the line width is afforded through inhomogeneous broadening by the application of constant B_0 gradients during spin-noise recording. This effect is demonstrated in the experiments shown in Fig. 4b. Homogeneous broadening due to the presence of paramagnetic CuSO_4 gives a qualitatively similar effect, as evidenced in Fig. 4c.

In Fig. 5, we compare spin-noise spectra of a sample of similar composition as in Fig. 1 under SNT0 conditions obtained on a cryo-probe (Fig. 5a) and on a room-temperature probe (Fig. 5b and c) to assess the influence of the temperature ratio ϑ . On the cryo-probe only the most intense signals (from the methyl groups) fulfill the condition for a "dip" spectrum due to the high proton density of 3.78×10^{28} spins m^{-3} for $(\text{CH}_3)_2$ at a concentration of 80%. The apparent spike near the center of the methyl doublet is unexpected and will be discussed below. Contrary to the behavior on the cryo-probe, all spin-noise peaks are "dips" for the same

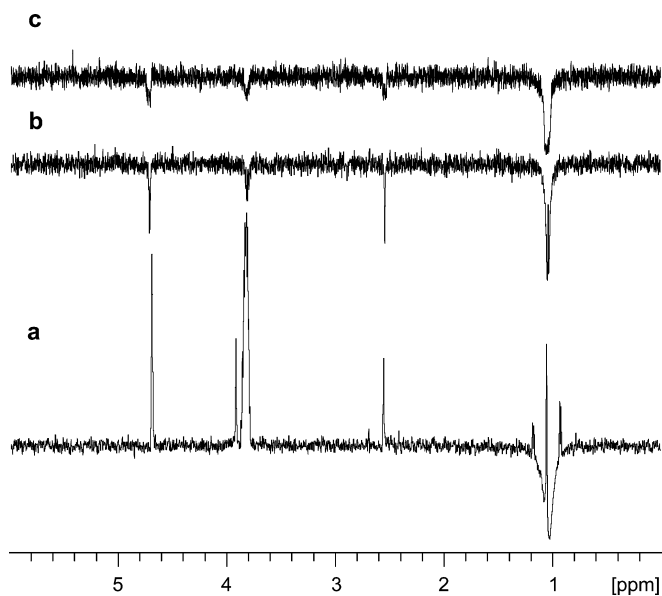


Fig. 5. Proton spin-noise spectra of the same sample as in Fig. 1 under SNTD conditions obtained on a 500 MHz cryo-probe (a) and on a 600 MHz room-temperature probe (accumulated from 4 K data blocks, b–c). A small static z-gradient was applied in spectrum (c) through variation of the spectrometer's z-shim current.

sample on a room-temperature probe, as can be seen in Fig. 5b. Application of a static field gradient, weakens and broadens the signals but does not give rise to any positive spin-noise component since $\vartheta = 1$ in Eq. (5), as illustrated in Fig. 5c. Note that the ^{13}C -satellites of the methyl protons are not observable with the room-temperature probe.

Simulations, some of which are shown below, support the experimental observations by showing that the effect of decreasing T_2 is a decrease of the negative broad component and an increase of the positive component, which first is narrower than the negative one but at higher relaxation rates exceeds its width. In situations where $T_2^* \ll T_{\text{rd}}$, a linear dependence of spin-noise power on spin concentration is found. These conditions were fulfilled in the experiments of Ref. [8].

McCoy and Ernst [4] have shown that by saturating the NMR signal prior to the recording of the noise spectrum the negative component of spin-noise can be removed. Saturation effectively increases spin temperature and a similar transitional behavior as for cryogenic probes can be observed following Eqs. (2) and (4) with $\vartheta > 2$. Leakage of rf-power makes obtaining pure spin-noise spectra requiring any form of rf-irradiation very difficult to execute, especially with highly sensitive receiver hardware.

4.3. Frequency shifts

On samples with narrow lines, we have observed frequency shifts of the spin-noise signals, that also depend on tuning and on the total amount of sample polarization. In Fig. 6a the concentration dependence of the spin-noise spectra observed on samples of acetone in benzene- d_6 is shown. While the positions and line shapes of the ^{13}C -satellites remain unaffected, a significant shift of the position of the central $^{12}\text{CH}_3$ -signals is observed. This effect is related to a similar one observed in pulsed spectra of concentrated spins in high Q probes [20]. The observed frequency shifts are adequately reproduced using Eq. (2) with $\Delta\omega_c \neq 0$ as shown in Fig. 7, and are very similar to the frequency shifts observed in small flip angle pulsed experiments in the presence of radiation damping. These shifts are related to the fact that the radiation damping reaction field is not

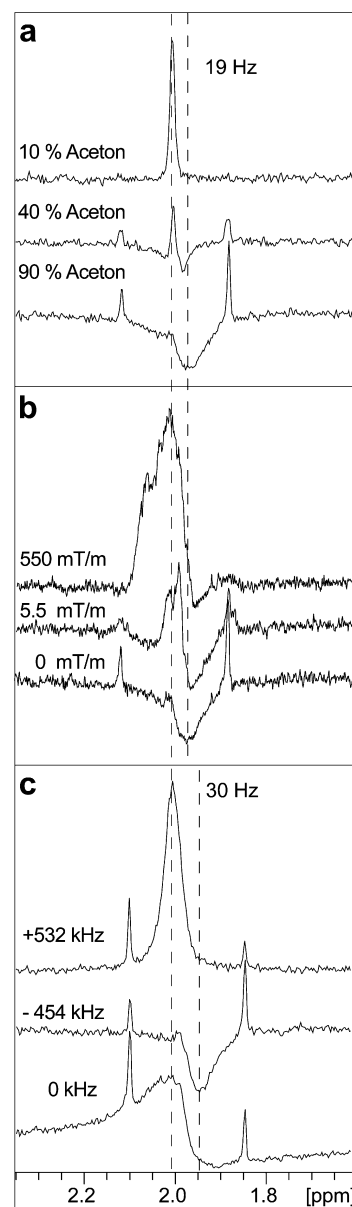


Fig. 6. Concentration dependence of spin-noise spectra of acetone in benzene- d_6 recorded on a 500 MHz cryogenic probe (a, 4 K accumulated noise blocks of 8 k data points). A reduction of the frequency shift is observed when applying weak z-gradients (b, 2 K accumulated blocks of 4 k data points) under otherwise identical conditions. When the tuning offset is varied (c, 4 K accumulated blocks of 8 k data points) the shape and position of the spin-noise signal change as discussed in the text.

exactly 90° out of phase if $\Delta\omega_c \neq 0$ [20]. The simulations drawn in Fig. 7a show the spin-noise line shapes of both the central peak and the ^{13}C -satellites and adequately reproduce the experimental spectra from Fig. 6a only if a small offset (20–30 kHz) from the SNTD is assumed as in the right column of Fig. 6a. For exact SNTD conditions there should not be a concentration dependent frequency shift in an ideal probe. In a non-ideal rf-resonator circuit the zero-frequency shift tuning position may not necessarily coincide with the spin-noise dip, increasing the complexity of the effects. Considering these prerequisites, the amplitude and sign changes upon application of gradients (Fig. 6b) and the frequency shifts observed upon tuning frequency changes (Fig. 6c) are sufficiently well reproduced by the simulations in Fig. 7b and c, respectively. The apparent over-emphasis of the ^{13}C -satellites can at least in part be explained by the reduction of the central peak intensity due to strong radiation

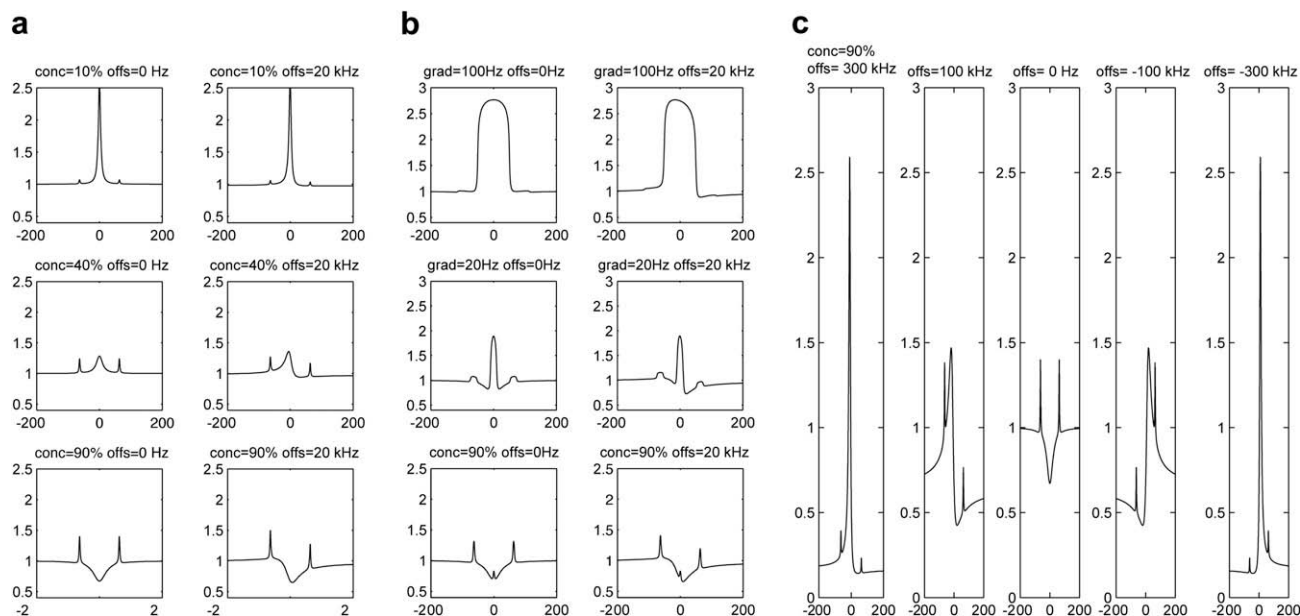


Fig. 7. Simulations of ^1H spin-noise spectra of acetone. In panel (a), we illustrate the concentration dependence; the second column of graphs takes into account a small tuning offset for better comparison with the experimental data of Fig. 6a. Panel (b), illustrates the dependence on B_0 gradient strength (indicated by the spread in Hz) of the 90% sample and should be compared to Fig. 6b. Again the right column simulates the realistic situation of a small tuning offset. In panel (c), the effects of large tuning offsets were simulated. Due to the non-ideality of the probe-circuit there is only a qualitative match with the experiments of Fig. 6c. The horizontal axes are labeled in Hz units relative to the central resonance frequency, while arbitrary units are used for the vertical axes.

damping broadening. On the other hand, radiation damping generally leads to a non-linear distortion of lineshapes [17], which is apparently also seen in these spin-noise spectra.

4.4. Complex line shapes

The methyl region of the iso-propanol spin-noise spectra in Figs. 1 and 5 presented a challenging problem for interpretation. In this case there is an intricate superposition of a spin coupled doublet, and the satellites due to the 1.1% ^{13}C nuclei. Assembling the spin-noise spectrum from six different Lorentzian shapes, and using Eq. (2), however, correctly reproduced the trends in the behavior under the various tuning conditions. In Fig. 8 we show the expanded methyl region under two different resonance offset conditions. Note that as a consequence of low M_z according to Eq. (3), the ^{13}C -satellites remain unchanged in position and line shapes while the superposition of the doublet components with their mixed line shapes gives rise to unexpected and unusual shapes that cannot easily be interpreted intuitively. A particularly puzzling observation is the appearance of a central spike as in Figs. 1, 5a and 8 and the shift of the broad peak with tuning, while the sharp spike at the center stays at the same frequency. The spin-noise simulations (red traces) superimposed in Fig. 8, however, follow the same trend. It is difficult to achieve a complete quantitative agreement between the simulations and the experiment, most probably because the properties of the resonance circuit deviate significantly from an ideal single oscillator behavior that is implicitly assumed in the derivation of Eq. (2) [2–4].

While the observed frequency shift and the appearance of a spike can be predicted rather reliably by simulating a coupled spin system in the presence of radiation damping in the small pulse flip angle regime [17], the sign changes in the spectral line shape are specific to spin-noise spectra only.

Although we can qualitatively explain the observed trends by Eq. (2), some deviations, in particular asymmetries in the spin-noise spectra as seen in Fig. 6 cannot be explained in a quantitative way. The discrepancies observed between the theory and our experiments are most probably due to the non-ideality of real

probe rf-circuits, which have to include more than the necessary minimum number of electronic components to meet the requirements of high resolution, high sensitivity multi-nuclear NMR spectroscopy. In particular, multiply tuned coils and rf-traps

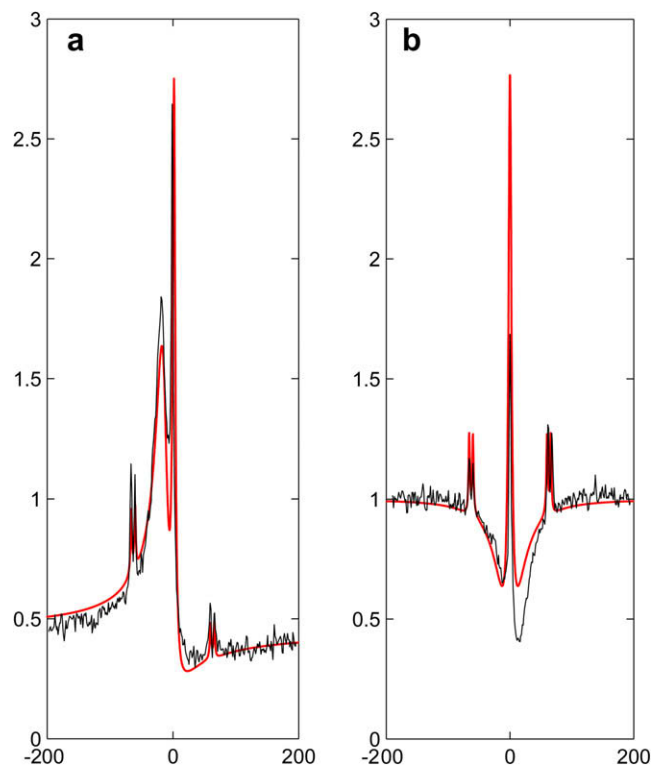


Fig. 8. Comparison of simulated and observed complex line shapes of the methyl doublet of the sample from Fig. 1 and Fig. 5. The black traces correspond to the experimental spectra, while the simulations are drawn in red color. The experimental tuning offsets $\Delta\omega_c^{\text{exp}}$ deviate from the simulated ones $\Delta\omega_c^{\text{sim}}$: (a) $\Delta\omega_c^{\text{sim}} = +150$ kHz, $\Delta\omega_c^{\text{exp}} = +407$ kHz, (b) $\Delta\omega_c^{\text{sim}} = 0$ kHz, $\Delta\omega_c^{\text{exp}} = -454$ kHz. The axes are labeled as in Fig. 7.

usually exhibit very irregularly shaped tuning curves like the one shown in Fig. 2. One of the most obvious consequences of this situation seems to be the large offset between the conventional tuning optimum and the SNT0. With such tuning curves (e.g., Fig. 2) no single quality factor Q will be sufficient to describe the circuit near resonance, and especially at larger offsets. Modifications to the Nyquist equations will have to be made to account for this non-ideality.

5. Conclusions

We have shown examples of ^1H spin-noise spectra recorded under a variety of conditions involving changes of probe tuning, application of gradients to assess the effect of inhomogeneous broadening, addition of paramagnetic agents to enhance homogeneous broadening and concentration. We showed that the complex interplay between radiation damping and relaxation leads to a non-linear amplitude response under the following general conditions: a high probe quality factor Q , a long transverse relaxation time, high spin density, and a large ratio between the sample's and the rf-circuit's temperatures. Non-linear behavior and complex line shapes of spin-noise signals can to a large extent be simulated using the formalisms introduced by Sleator et al. [3], McCoy and Ernst [4] as well as Guéron [6] with the notable exception of a probe-dependent offset between the tuning frequency of the rf-circuit and the spin-noise tuning optimum (SNT0). The ^{13}C -satellites observed here appear largely undistorted and do not experience frequency shifts, although it is puzzling to see their amplitudes overemphasized compared to the main signal. The fact, that one can relatively easily detect such small signals, gives a positive outlook on the possibility to observe small spin numbers through spin-noise based detection. In addition, we believe that spin-noise phenomena can become very useful for design goals and testing procedures of magnetic resonance rf-probes and for performance optimizations. For example, the determination of exact tuning conditions as suggested by Huang et al. [20] using the radiation damping reaction field is related to adjusting for SNT0 conditions as presented here and in Ref. [19] with an exact dip in the noise spectrum. The spin-noise tuning technique may be simpler, since no reference spectra have to be recorded, and no transient phase shifts have to be taken into account.

Acknowledgments

This work was supported by the FWF (Austrian Science Funds) Project No. P19635-N17 (to N.M.), the ÖAD (WTFZ AT-HR, to N.M.), a

grant to A.J. by the US NSF (CHE-0550054), and by the Croatian Ministry of Science, Education and Sports (project 098-0982929-2917, to V.S.). We acknowledge inspiring discussions with C. Anklin, A.D. Bain, W. Bermel, G. Gray, and T. Sleator.

References

- [1] F. Bloch, Nuclear induction, *Phys. Rev.* 70 (1946) 460–475.
- [2] T. Sleator, E.L. Hahn, C. Hilbert, J. Clarke, Nuclear-spin noise, *Phys. Rev. Lett.* 55 (1985) 1742–1746.
- [3] T. Sleator, E.L. Hahn, C. Hilbert, J. Clarke, Nuclear-spin noise and spontaneous emission, *Phys. Rev. B* 36 (1987) 1969–1981.
- [4] M.A. McCoy, R.R. Ernst, Nuclear spin noise at room temperature, *Chem. Phys. Lett.* 159 (1989) 587–593.
- [5] M. Guéron, J.L. Leroy, NMR of water protons. The detection of their nuclear-spin noise, and a simple determination of absolute probe sensitivity based on radiation damping, *J. Magn. Reson.* 85 (1989) 209–215.
- [6] M. Guéron, A coupled resonator model of the detection of nuclear magnetic resonance, radiation damping, frequency pushing, spin noise, and the signal-to-noise ratio, *Magn. Reson. Med.* 19 (1991) 31–41.
- [7] S.A. Crooker, D.G. Rickel, A.V. Balatsky, D.L. Smith, Spectroscopy of spontaneous spin noise as a probe of spin dynamics and magnetic resonance, *Nature* 431 (2004) 49–52.
- [8] N. Müller, A. Jerschow, Nuclear spin noise imaging, *Proc. Nat. Acad. Sci. USA* 103 (2006) 6790–6792.
- [9] P. Messina, M. Maninni, A. Caneschi, D. Gatteschi, L. Sorace, P. Sigalotti, C. Sandrin, S. Prato, P. Pittana, Y. Manassen, Spin noise fluctuations from paramagnetic molecular surfaces, *J. Appl. Phys.* 101 (2007) 053916, 1–14.
- [10] H. Kovacs, D. Moskau, M. Spraul, Cryogenically cooled probes—a leap in NMR technology, *Prog. Nucl. Magn. Reson. Spectrosc.* 46 (2005) 131–155.
- [11] L. Darrasse, J.-C. Ginfri, Perspectives with cryogenic RF probes in biomedical MRI, *Biochimie* 85 (2003) 915–937.
- [12] D.I. Hoult, N.S. Ginsberg, The quantum origins of the free induction decay and spin noise, *J. Magn. Reson.* 148 (2001) 182–199.
- [13] D.I. Hoult, B. Bhakar, NMR signal reception: virtual photons and coherent spontaneous emission, *Conc. Magn. Reson.* 9 (1997) 277–297.
- [14] H. Nyquist, Thermal agitation of electric charge in conductors, *Phys. Rev.* 32 (1928) 110–113.
- [15] X.-A. Mao, C.-H. Ye, Understanding radiation damping in a simple way, *Conc. Magn. Reson.* 9 (1997) 173–187.
- [16] W.S. Warren, S.L. Hammes, J.L. Bates, Dynamics of radiation damping in nuclear magnetic resonance, *J. Chem. Phys.* 91 (1989) 5895–5904.
- [17] A. Vlassenbroek, J. Jeener, P. Broekaert, Radiation damping in high resolution liquid NMR: a simulation study, *J. Chem. Phys.* 103 (1995) 5886–5897.
- [18] M.P. Augustine, Transient properties of radiation damping, *Prog. Nucl. Magn. Reson. Spectrosc.* 40 (2002) 111–150.
- [19] D.J.-Y. Marion, H. Desvaux, An alternative tuning approach to enhance NMR signals, *J. Magn. Reson.* 193 (2008) 153–157.
- [20] S.Y. Huang, C. Anklin, J.D. Walls, Y.-Y. Lin, Sizable concentration-dependent frequency shifts in solution NMR using sensitive probes, *J. Am. Chem. Soc.* 126 (2004) 15936–15937.